PERGAMON

International Journal of Heat and Mass Transfer 42 (1999) 2129–2142

International Journal of HEAT and MASS TRANSFER

Estimation of thermal contract resistance during the first stages of metal solidification process: II—experimental setup and results

T. Loulou*, E.A. Artyukhin, J.P. Bardon

Laboratoire de Thermocinétique, I.S.I.T.E.M., La Chantrerie, BP 90604, F-44306, Nantes, France

Received 19 October 1998

Abstract

This paper presents an experimental study of transient heat transfer in the early stages of solidification of some pure metals on water cooled substrate, quantified in terms of two parameters: thermal contact resistance at the interface and heat flux. Experiments were performed to measure the thermal contact resistance during solidification of tin, lead and zinc drop on nickel substrate. The study is focused on the heat transfer aspects of this process and the identification of parameters affecting the heat transfer mechanism. To this end, the influence of casting process variables such as substrate surface roughness, casting material, metal superheat and lubricant on heat transfer has been analyzed.

Nomenclature

C_p heat capacity
L latent heat
R_a surface roughness
$\mathscr{R}(t)$ thermal contact resistance
r contact radius
St Stefan number
ΔT superheat
T temperature
$T_c(a,t)$ casting surface temperature
$T_s(a,t)$ substrate surface temperature
t_c time delay.

Greek symbols
α thermal diffusivity
λ thermal conductivity
μ dynamic viscosity
ρ density
σ surface tension
θ contact angle
$\varphi(t)$ heat flux.

Subscripts
c casting
Ch chromel
Ni nickel
s substrate.

Superscripts
i initial
m melting.

1. Introduction

In the companion paper, we have shown that heat transfer through the melt/mold interface is an important aspect of the solidification of materials which is of particular interest in materials processing, metallurgy, purification of metals, continuous casting and other various solidification operations. Previous studies, presented in the companion paper, have demonstrated that heat extraction from the casting is controlled by the casting/mold interface. The fundamental mechanisms that control the thermal contact between a solidifying molten metal and the mold wall are not well understood. The thermal behavior of the interface is characterized by the

* Corresponding author. E-mail: loulou@isitem.univ-nantes.fr

0017–9310/99/$ - see front matter
PII: S0017–9310(98)00338–X

thermal contact resistance coefficient which is known to vary with time and along the mold/casting interface. Several numerical and experimental results indicate that the interfacial thermal conductance is indeed often the controlling factor of the solidification rates which in turn determine the properties of the produced materials. On the other hand, the quality of solidified metal depends on the thermal conditions evolution during solidification.

When studying the thermal behavior of the casting/mold interface, many experimental and numerical studies consider the steady state case of the interfacial resistance while others consider the unsteady state. To differentiate the two cases, one must consider the ratio between the time required to form a stable shell and the total time of casting solidification. If the ratio is about 1, the unsteady nature of the interfacial resistance must be taken into consideration. In the case of continuous casting of the thin flat products, the unsteady state of the thermal contact resistance between casting and mold must be considered.

As mentioned before, the measurement of this thermal contact resistance is challenging, and few experimental data are available in the literature. Using temperature measurements in both casting and mold, several studies [1–10] have attempted to quantify the transient interfacial heat transfer during solidification. All these authors have discussed the physical mechanisms of the interfacial resistance development due to imperfect contact between the solidifying metal and the mold. They have also investigated the influence of casting parameters such as superheat, mold materials, melt materials, mold geometry and surface roughness, contact pressure, mold coatings, initial temperature of mold and casting and thermophysical properties of both media, on the interfacial heat transfer and the cast quality (microstructure of the solidified material).

Many types of heat extraction devices are used in near net shape continuous casting of flat products: single roll, twin roll, twin belts, etc. [11]. In the case of the single roll device, molten metal is allowed to solidify directly on a solid wall (substrate). To study the evolution of thermal contact conditions in this kind of device, we simulate the casting process by the fall of a liquid metal drop on a solid substrate [12]. All previous cited studies indicate that the most important part of heat extraction takes place in the first stages of thermal contact. To get thermal information ($0 < t < 1$ s), local and accurate measurement tools are prepared in both sides: solidifying drop and substrate [12].

The experimental work developed here focuses on transient heat transfer in the first stages of solidification of pure metals on water-cooled substrate under various conditions. The first objective was to experimentally investigate the thermal contact evolution in terms of interfacial thermal conductance and heat flux, and the influence of process parameters such as initial melt temperature, thermophysical properties of casting, substrate surface roughness, lubrication at the interface and superheat of the molten metal.

2. Experimental setup

To analyze the thermal contact resistance occurring at the interface between the metal casting and the mold, an experimental investigation is conducted. As explained in Ref. [12], the experiment consists of a falling molten metal drop on an implemented substrate. For this purpose, an experimental set up, shown in Fig. 1, was realized. It is constituted of three main parts.

The first part is an electric mini-furnace to melt and to preserve the liquid metal at high temperature. The temperature regulation is allowed by a thermocouple installed in the lower part of the furnace. At the center of this lower part, an electromagnetic shutter can be opened to ensure the sudden falling of the liquid metal on the center part of the substrate.

The second part is the wall which receives the molten metal drop. The wall has a cylindrical shape of 50 mm in diameter and 10 mm in height. It is essentially constituted of two layers. The first one is in nickel (3 mm). The second layer is in copper (7 mm). The nickel layer which constitutes the substrate of the metal drop, is deposited by electrolytic process on the copper layer. The copper layer is maintained on support which is regulated in temperature by a thermostatic water circulation. The surface state of the nickel layer is carefully chosen in order to investigate the effect of roughness on thermal contact resistance.

Four semi-intrinsic micro-thermocouples (each one constituted of one wire of 25 μm in diameter) are planted carefully in the nickel layer along its axis. For an accurate implementation of the wires, the substrate is cut along an axial symmetric plane, in two parts. On one of these parts and at different depths ($X_{\min} < x_i < X_{\max}$) from the active surface, each wire is soldered on its end on the center line and placed in a thin crack parallel to the nickel surface to minimize the heat drain. The exact position of the sensor junctions with respect to the active surface, given in Table 1, are measured by an optical profilometer before the two parts are precisely re-assembled. The molten metal drop comes on the center of the nickel surface and covers a thermocouple stretched parallel to the nickel surface. The exact position of this thermocouple (see Table 1), is measured after the experiment by cutting the solidified metal drop. The height of fall is chosen to avoid drop bursting during the fall. The drop and the substrate are shown in Fig. 1.

To verify precisely the position of the measurement point inside casting, the solidified drop is cut in two parts and the thermocouple junction is located in the solidified metal. Then the distance is measured with respect to the

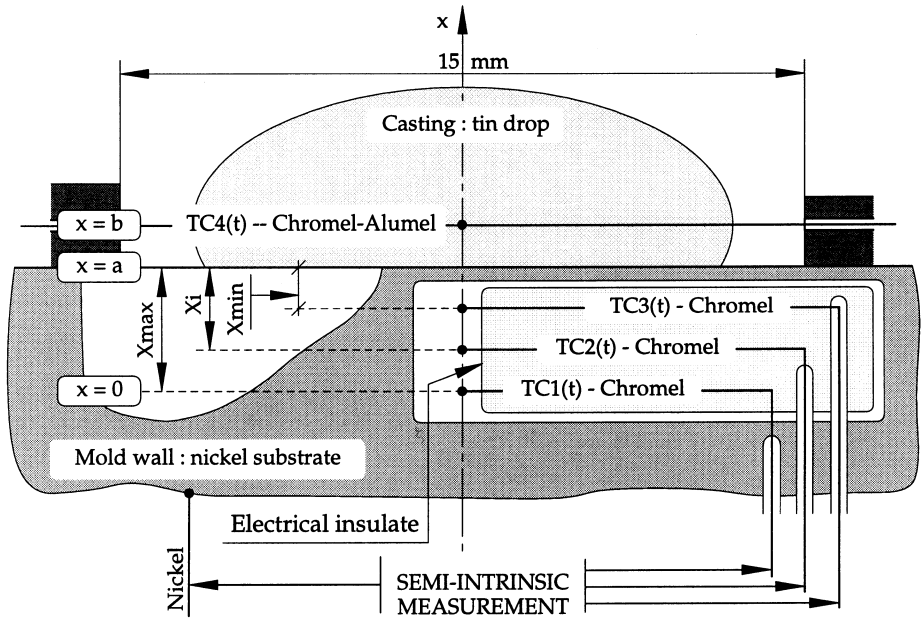

Fig. 1. Experimental setup.

Table 1
Roughness and thermocouple positions with respect of the contact interface in μm

	TC_1	TC_2	TC_3	TC_4	TC_5	Casting	Roughness R_a
Substrate 1	—	188	328	481	1007	1200	0.33
Substrate 2	136	255	373	510	625	1200	0.66
Substrate 3	—	191	360	458	740	1200	15.58

bottom surface (contact surface). During our experiment tests we observed a small displacement of the measurement point inside the casting and the error is about 3–5%.

The third part is a cooled radiation shield which is placed before the drop falling between the furnace and the substrate to eliminate any radiation between them.

2.1. Principle of the substrate surface temperature measurement

Many different methods have been developed for measuring surface temperature in heat and fluid flows [13]. Unfortunately, the accurate direct measurement of a surface temperature is very difficult. The implementation of sensors at the active surface causes perturbations which result in significant heat disturbances.

An alternative way to eliminate the thermal disturbance is to develop indirect measurements. The principle consists in using measured temperature inside the body, immediately underlying the active surface, (see Fig. 1), and at different depths ($X_{min} < x_i < X_{max}$), to determine the surface temperature by extrapolation of different theoretical or empirical laws. This method presents a good advantage because the imbedded sensors are less perturbed than a surface sensor and they do not disturb the measurements of the surface temperature. But this method is very sensitive to the errors on the sensor locations and formally mainly applies to steady phenomena.

Recently, great progress in inverse heat conduction analysis allows its use in various unsteady heat transfer phenomena, and in particular those being developed from the active surface body to the back side. The inverse method used in our case is described in detail in the companion paper [12].

2.2. Semi-intrinsic thermocouple measurement

The principle of the semi-intrinsic method [14, 15] consists in using the material itself as one thermocouple element (string chromel; see Fig. 1). Consequently, the

semi-intrinsic method can be applied only on electrically conducting materials. Sensors are constituted of a thin string (chromel) embedded in the nickel substrate on the vertical axis of the wall. The different strings of chromel metal are situated parallel to the active surface to minimize the heat losses. The surface of the wire is electrically insulated from the nickel metal. The choice of the chromel metal leads to the maximum sensitivity of the metal couple chromel-nickel. This kind of thermocouple presents several advantages:

- The thermocouple inertia is very low. It is extremely important in the case of transient phenomena. The time delay is of the order of the characteristic time of the micro-constriction establishment phenomenon. It can be shown, that this time delay, at 97% is given by:

$$t_c = \frac{100r^2}{\alpha} \quad (1)$$

  where r is the junction size (equal to the radius of the chromel element) and α the thermal diffusivity of the nickel medium. The best performance is obtained for a string (chromel metal) with the lowest radius ($\phi 25$ μm was chosen in building the sensor). For the case of our experiment the time delay is about $t_c < 10^{-4}$ s.
- The error of temperature measurement is about 0.025°C which is considerably reduced in comparison with the error introduced by a classical thermocouple with two wires.
- The heat losses are divided by two, and the influence of thermal contact resistance between nickel medium and chromel sensor is reduced in the ratio $\lambda_{Ni}/(\lambda_{Ch}+\lambda_{Ni})$. So that the error is globally divided by $\lambda_{Ni}/2(\lambda_{Ch}+\lambda_{Ni})$.

The disadvantages of the semi-intrinsic thermocouple are essentially the need for in situ calibration, the risk of significant electric noise and the difficult arrangement of the wire in the thin wall partly due to the small distance from the active surface.

3. Experiments

The first experiments are conducted using a pure metal: pure tin on a nickel substrate. The molten metal falls freely, as a drop, on the solid substrate at room temperature. The fall height is equal to 1.5×10^{-2} m. The weight of the molten metal is 3.5×10^{-3} kg. As explained in [12], during the drop fall, the stretched thermocouple near the substrate surface is drowned in the solidifying metal. When the molten metal drop touches the substrate, it becomes flat at its lower part. At the end of the solidification process, the drop looks like a portion of a sphere. Using a CDD camera, we have visualized the flow of the molten metal during its impact on the substrate. In the first stages of the contact, the molten metal spreads on the substrate. The spreading process is stopped when the viscous forces equilibrate the kinetic ones, acquired during the liquid metal fall, and solidification starts from the side surface. Then the remaining molten metal gets accumulated in the middle of the splat and forms a portion of a sphere at the end of the flow and solidification processes. The size of the solidified metal drop is about $10–11 \times 10^{-3}$ m in diameter and $4–5 \times 10^{-3}$ m in height. Our experiments are conducted on substrates of three different roughnesses, all of them in the nickel.

In the following section, we first discuss a typical experimental measurement profile. These measurements recorded in the casting and substrate regions are shown in Fig. 2. In this specific case, the initial temperature of casting and substrate are respectively 300 and 20°C. Tests are conducted in the ambient room (interstitial fluid: air) and on the third substrate ($R_a = 15.58$ μm). The first four thermocouple recordings correspond to measurements in the substrate region. The fifth one matches the measurement done in the casting region. In the substrate region, the temperature measurements quickly reach a maximum value, once the contact is established with the liquid metal, and then decrease slowly close to room temperature. This result is similar to that observed in the literature [16, 17, 4]. The substrate is heated by the melt superheat transferred from the casting to the substrate through the interface and by the latent heat of solidification.

Local heat flux and thermal contact resistance between the substrate and the solidifying metal are estimated by solving the appropriate heat transfer problem in both regions. One dimensional heat transfer is assumed in the substrate and casting regions because of the very close distances between sensors and the surface. The formulation and numerical solution procedure used in this model is described in detail in our previous paper [18].

The source of errors is estimating the parameters which define the evolution of the thermal contact conditions are different: temperature measurement, thermocouple locations, thermophysical properties of medium, estimation procedure, etc. A detailed error analysis, shows that the estimation error of $T_c(a,t) - T_s(a,t)$, $\varphi_{int}(t)$ and $\mathscr{R}(t)$ are respectively about 6, 6 and 12%.

3.1. Validation of the inverse method

In the first stage, temperature measurements inside the substrate are used to validate the inverse heat conduction algorithm. This validation consists of estimating the temperature evolution at the location of the fourth thermocouple. To do that temperature readings of the other three thermocouples are used as an additional information. The comparison shows a good agreement between measured and estimated temperature. The validation test and the estimated substrate surface temperature are shown in Fig. 3.

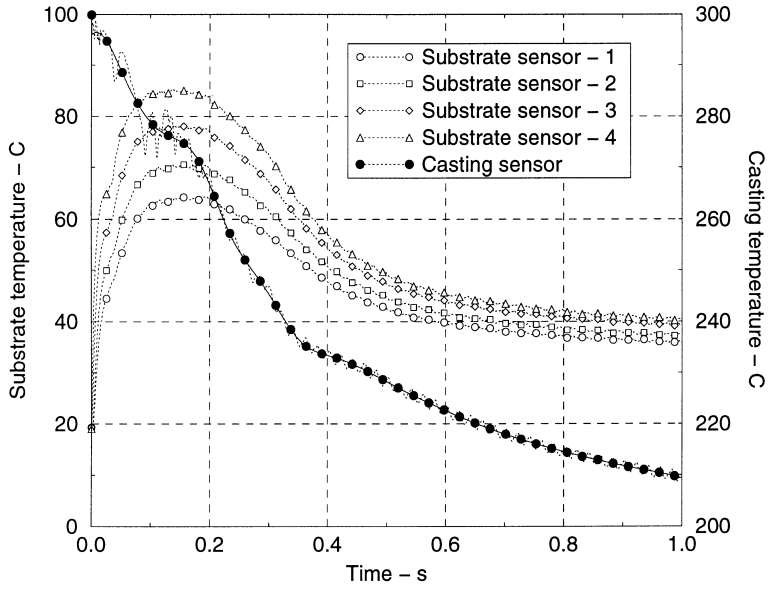

Fig. 2. Measured temperatures.

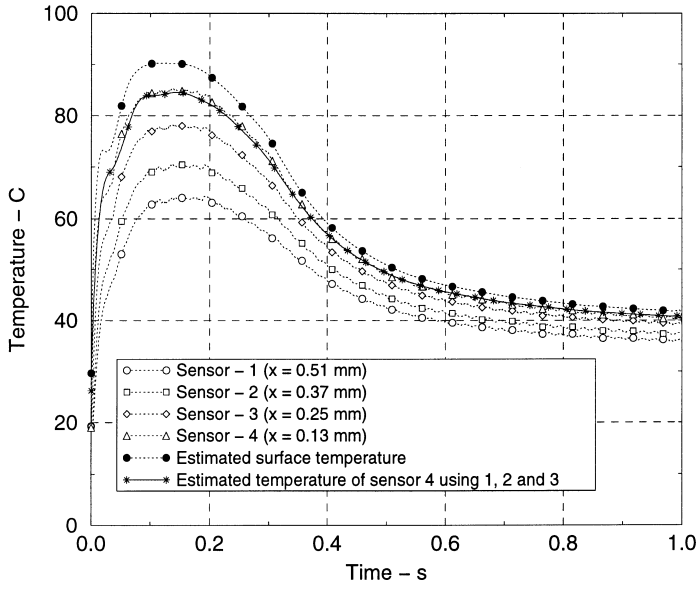

Fig. 3. Temperature evolution in the substrate side.

The temperature evolution at the bottom layer of the drop (interface) and at the measurement point installed in the casting region is shown in Fig. 4.

The evolution of the thermal contact resistance at the interface is shown in Fig. 5. The time-dependent resistance is given by the ratio between the temperature jump and the heat flux at the interface. After quickly decreasing in the first stages of contact, the thermal resistance stabilizes a short moment and then starts to increase slowly. In the following section, we try to characterize its time evolution in four principal steps **A**, **B**, **C** and **D**. A schematic representation of the solidification process during the three main steps is shown in Fig. 6.

The first stage **A** is characterized by a very quick decrease due to some factors occurring during the drop fall: As the melt spreads on the substrate, the contact surface increases. In the beginning of the process, the melt-substrate contact is better because the melt is still

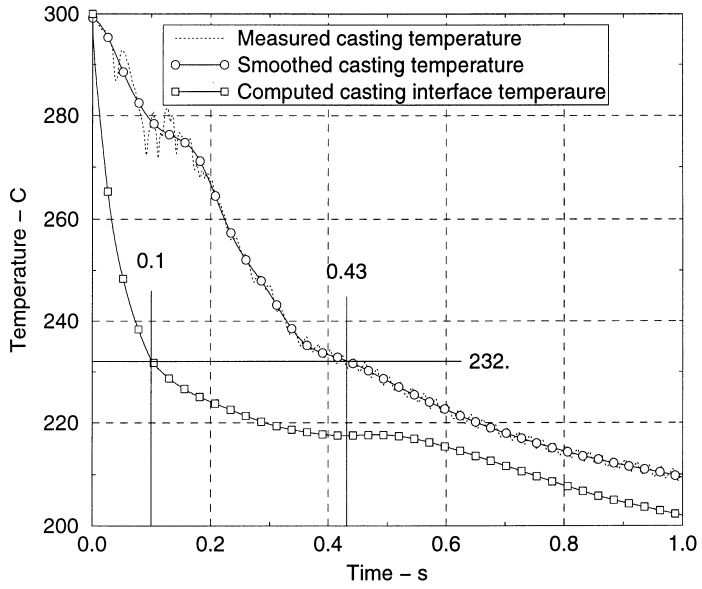

Fig. 4. Temperature evolution in casting.

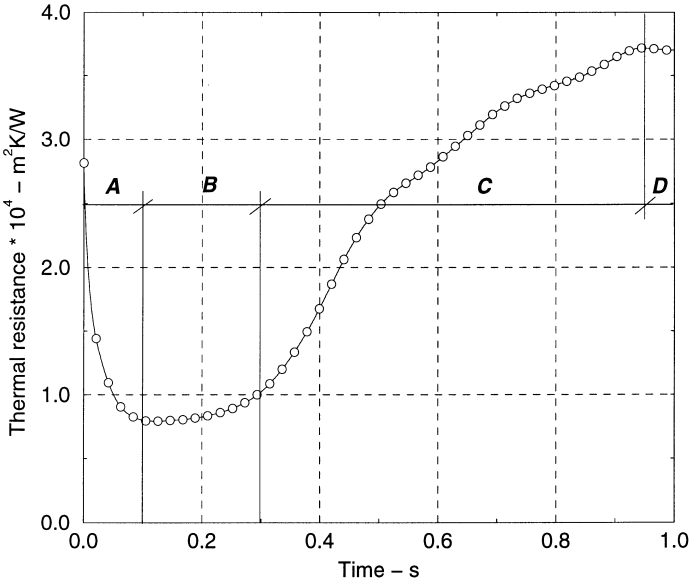

Fig. 5. Evolution of thermal contact resistance at the interface.

liquid. In this stage, the molten metal is in contact with the substrate, just through the roughness picks. The superheat is removed, mainly by conduction, throughout the contact areas. The interstitial air is eliminated progressively but not completely. A small volume remains trapped in the roughness microcavities. Then an equilibrium is established between the surface tension of the liquid and the trapped air pressure. The liquid metal tends to maintain a better thermal contact with the substrate which explains the weak value of thermal contact resistance.

During step **A**, thermal contact resistance is a function of the substrate roughness, surface tension of the liquid metal, wettability and the contact angle of the surface, nature of the trapped gas and pressure of liquid metal.

At the end of this stage, the wetted surface and heat flux are maximum. Thermal contact resistance is minimum. The thermal contact is established just on the

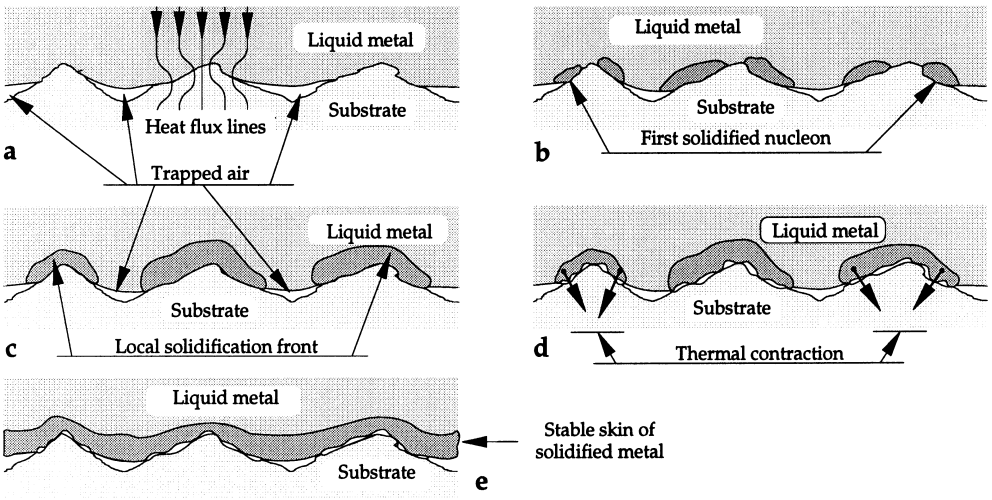

Fig. 6. Schematic representation of the solidification process evolution at the interface.

roughness picks and from these contact areas starts the solidification process. The nucleation begins, precisely, from the triple line contact (molten metal, substrate surface, trapped air) where the temperature is the lowest. Step **A** corresponds to Fig. 6(a).

Step **B** is characterized by a quasi-stability of thermal contact resistance around a minimum value. Around each local roughness pick, the nucleation phenomenon continues to progress and forms around the roughness pick a solidified ring (see Fig. 6(b)). As there are numerous contact zones, we have as much local solidification fronts. On the other hand, there are a lot of local small solidification fronts. At this stage of the phenomenon, we have an almost equal-distribution in the crystal growth orientation. The ring grows and its inner diameter decreases to zero. Finally the roughness pick is completely covered by a solidified cap of metal, Fig. 6(c). As, the solidified cap increases, the resulting thermal gradient is more important. Then the metal contracts from the roughness peak because of volume change upon solidification and simultaneously and the roughness peak expands. As a result, it generates a shear strain at the contact interface of the solidified cap and roughness peak (see Fig. 6(d)). On the other hand, the interfacial gap grows due to thermal contraction of casting and the mold expansion. As a consequence, thermal contact resistance starts to increase slowly. At the end of this step, all the local fronts unite and form an unique solidification front, Fig. 6(e). Then a fine stable crust of solidified metal is formed and shrinkage phenomenon becomes more important.

Step **C** is characterized by regular growing of thermal contact resistance. The thickness of solidified metal crust increases progressively and contracts from the substrate which increases in the same time the size of the interfacial gap. The important temperature gradient in the solidified crust causes its shrinkage from the substrate surface. The width of contact zones and their number is reduced gradually. The interfacial gap tends to be stable when the solidified crust metal is sufficiently thick. Then the interface contact is reduced to a solid—solid contact. The end of this step is distinguished by a stabilization of thermal contact resistance which corresponds to the beginning of the **D** step.

Step **D** characterizes the end of the transient state of thermal contact resistance. The solidified metal crust is thick enough and the contact is reduced to a stabilized solid-solid contact. The heat transfer is a function of temperature, coating film, oxide films at the interface and pressure if the solidified metal and mold are under pressure.

During the four stages **A**, **B**, **C** and **D**, the heat transfer at the interface is by conduction through contact peaks between the substrate and casting, conduction through the trapped gases in the interfacial gap and radiation between the surfaces forming the gap. Heat transfer by radiation is more important when the temperatures are high.

3.2. Roughness surface analysis and effect of lubricant type

To precisely analyze the common contact surface of the melt and the substrate, we have analyzed the roughness on two facing parts of the contact. This analysis allows us to see the effect of the substrate roughness, surface tension and wettability on the thermal contact resistance evolution. The roughness of solidified metal must represent in the negative the substrate roughness.

The surface roughness was determined with an optical

surface roughness analyzer (UBM) that is able to measure both the roughness and waviness components of the surface texture. The roughness is given in terms of the arithmetic mean of the departures of the amplitude profile from the mean line (R_a in μm) which is the most used international parameter of roughness. The characteristics of the analyzer are: measurement resolution 20×10^{-9} m, measuring spot diameter 1 μm, measurement range ± 50 μm.

The roughness analysis is bidimensional and done upon a square of 2 mm of side. The analysis resolution is 1000 point per mm. We note that the surfaces on both sides are not isotropic. The mean roughness parameter is $R_a = 15.58$ μm for the substrate while the mean roughness of the solidified metal is $R_a = 12.27$ μm. The solidified metal approximately replicates the substrate texture. We observed a clear difference between the two surface morphologies. The solidified metal surface is smoother than the substrate one and shows that the wettability, which depends on surface tension, is not perfect and that gases are still trapped in the bottom of the roughness microcavities. Moreover, the shrinkage phenomenon in the solidified metal and the thermal expansion of the substrate tend to separate two surfaces in contact. The effective heat conduction surface (throughout liquid or/and solid–solid contact) is smaller than the nominal contact surface. This analysis will be used in the future to build a contact model and to precisely determine the contact surface.

We conducted different tests, with the same experimental conditions, on three substrates presenting a different roughness, and with different interstitial mediums, gas (air) or film coating (oil, grease). The effect of an interfacial medium on heat flow in terms of the evolution of heat flux and thermal contact resistance is shown in Figs. 7 and 8. These results are obtained using the rougher substrate ($R_a = 15.58$ μm). Table 2 presents the results of the different test cases. The nature of the lubricant seems to influence the heat transfer rate at the casting-substrate surface. The presence of oil or grease at the interface contributes to improve the heat transfer rate by minimizing the effect of numerous microcavities filled by air. It is seen that there is a general enhancement in the heat flux and heat transfer rate when the interfacial medium is a better thermal conductor than air.

For the other tests, corresponding to lower roughness substrates ($R_a = 0.30$ μm and $R_a = 0.66$ μm), we observed that the solidified metal is rougher than the substrate. This result is opposite to the result for a large value of the surface roughness ($R_a = 15.58$ μm). A similar behaviour was observed by Muojekwu et al. and Prates et al. [19, 4]. This means that between these should exist a critical roughness value $(R_a)_{cr}$ for which this change of behavior occurs. In Fig. 9, we have plotted the time evolution of the thermal contact resistance as a function of substrate roughness (in the case of air as an interstitial medium). We observe that when the roughness decreases, the thermal contact resistance decreases, leading to an improvement in the heat transfer rate.

3.3. Effect of melt superheat

To see the melt superheat effect on thermal contact conditions, we conducted a series of tests, on the same

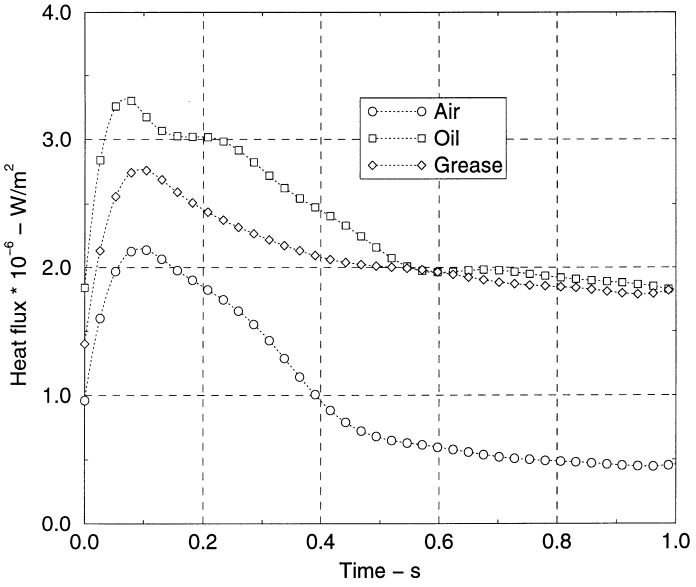

Fig. 7. Evolution of heat flux vs the substrate coating for a roughness = 15.58 μm.

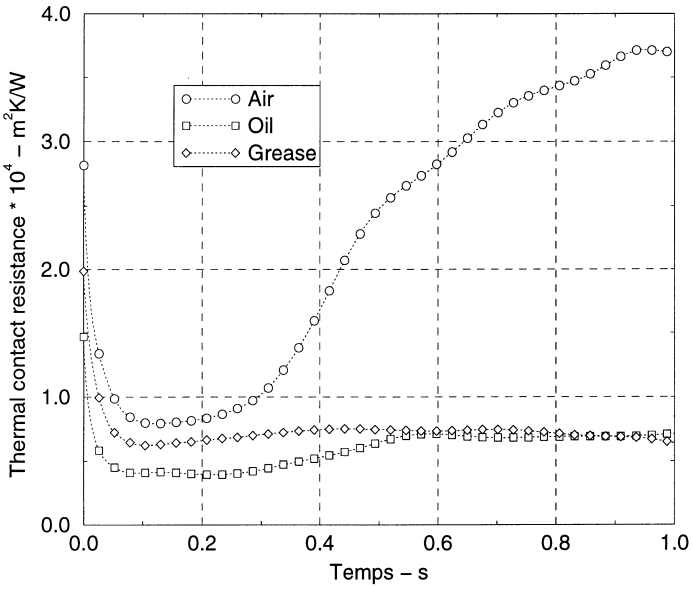

Fig. 8. Influence of coating film on thermal contact resistance.

Table 2
Comparison between substrate roughness and solidified metal roughness vs film coating

Film coating	Substrate 1 $R_a = 0.30$	Substrate 2 $R_a = 0.66$	Substrate 3 $R_a = 15.58$
Air	1.10	1.42	12.27
Oil	—	0.81	3.66
Grease	—	4.02	5.87

substrate ($R_a = 15.58$ μm) and with the same experimental conditions. The evolution of thermal contact resistance as a function of superheat is presented in Fig. 10. Results are presented with three different melt superheats. In general, thermal contact resistance presented approximately the same evolution as before. We observe that when the superheat of the casting increases, heat flux grows and thermal contact resistance decreases. This behavior can be readily understood from the variation in slowness of the cooling of solidified metal.

The results of surface roughness measurements of solidified metal are presented in Fig. 11 as a function of metal superheat. Measurements of surface roughness of the solidified metal indicate that it reaches the substrate one as superheat increases for the same substrate surface microprofile. This means that the surface contact is increased, thereby leading to higher heat transfer rate. When the superheat is higher, the molten metal fluidity is increased and its spreading on the substrate is better. In conclusion, the higher the melt superheat, the better the liquid metal substrate contact and heat transfer rate and the lower the thermal contact resistance.

3.4. Effect of the casting nature

To investigate the effect of the casting nature, three materials are used: tin, lead and zinc covering a wide range of thermophysical properties as shown in Tables 3 and 4. These experiments are conducted without any lubricant at the interface (in ambient air). The initial melt temperatures are given in Table 4.

The time evolution of the heat flux at the interface is shown in Fig. 12. The temperature jump at the interface, for the three materials is shown in Fig. 13. Its evolution as a function of time is approximately the same. The temperature jump decreases quickly in the first stages corresponding to step **A** of the evolution of thermal contact resistance, described previously. A more important temperature drop is observed in the case of zinc.

The evolution of thermal contact resistance as a function of time corresponding to three materials is shown in Fig. 14. Step **B** is approximately the same. The period of liquid metal contact is still similar in the three cases. Step **B** is the same just for the tin and zinc. Lead presents a shorter step **B** than tin and zinc, due to its weak latent heat. On the other hand, lead gets cooled faster. This establishment is extended to step **C** compared to the others. The cooling rate is more important and a constant value of thermal contact resistance is rapidly reached. In the zinc case, the thermal contact resistance increasing (step **C**) is slow in comparison with tin and lead. An underlying cause of slowness in growth is probably its very important latent heat.

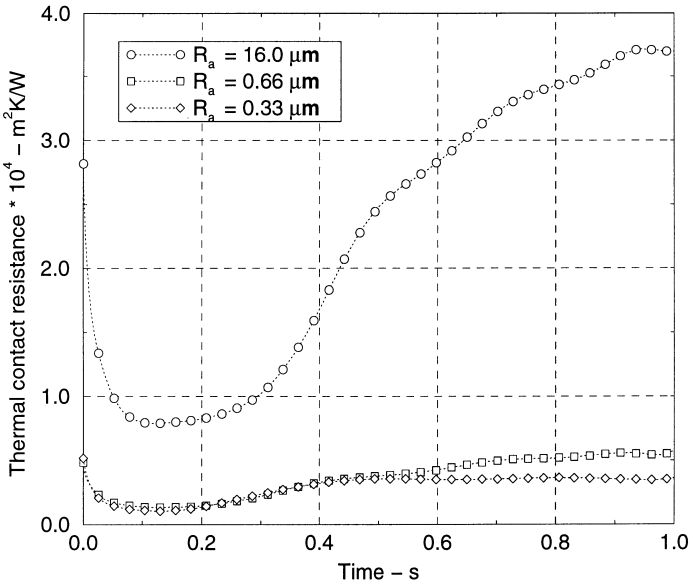

Fig. 9. Thermal resistance evolution vs substrate roughness.

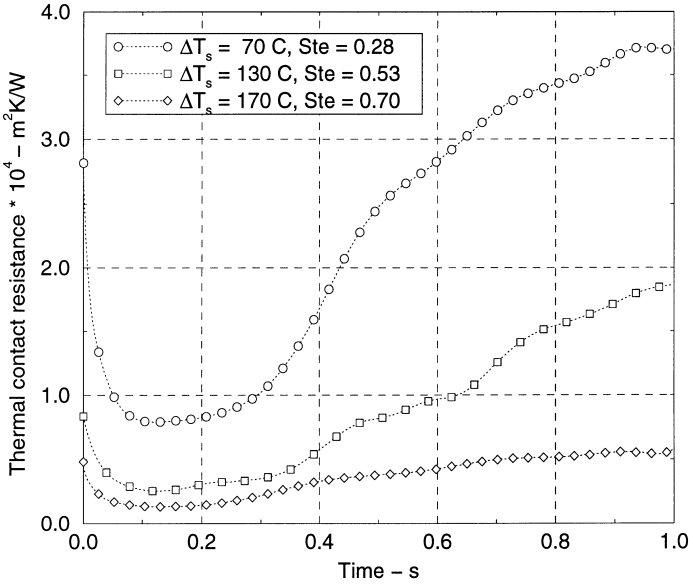

Fig. 10. Thermal resistance evolution for different superheat values.

Table 4 shows the physical data related to the contact conditions of the materials used in this study [20]. The roughness analysis of the three solidified materials is also given in Table 4.

Regarding the surface roughness analysis and the three drops morphology, the material which has the lowest surface tension and the lowest contact angle (see Table 4) presents the nearest surface roughness to the substrate one. This result suggests that the quality of the contact depends of the surface tension and contact angle of the melt.

The dynamic viscosity at melting temperature (given in Table 4) is approximately the same for the materials. This means that their falls and flowing on the substrate surface is similar and do not affect the contact quality. This result is proved by the same evolution of thermal contact resistance in the first stages of contact.

Another interpretation of these results could be found

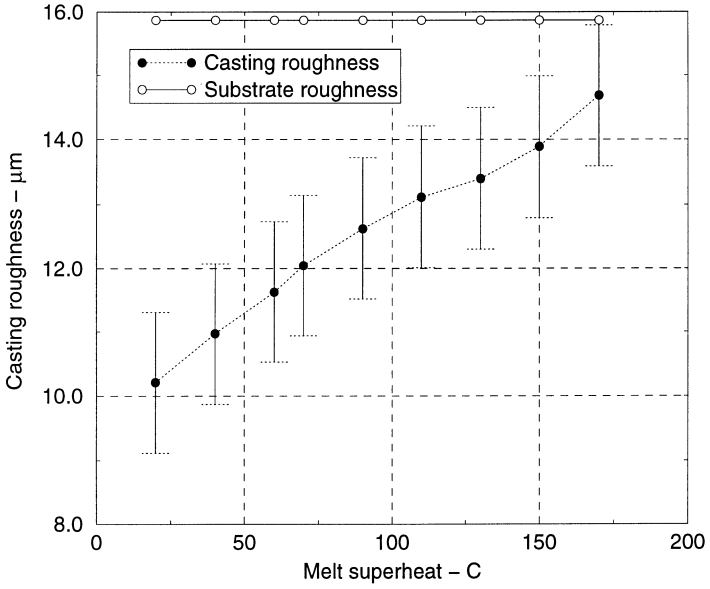

Fig. 11. Evolution of casting roughness vs the superheat parameter.

Table 3
Thermal conductivity and heat capacity of used materials

Nature of metal	Thermal conductivity		Heat capacity	
	Solid	Liquid	Solid	Liquid
Tin	$65.54-0.025T$	$25.54+0.020T$	$223.521+0.15T$	$271.68-0.094T$
Lead	$35.20-0.013T$	$10.35+0.016T$	$127.97+0.043T$	$152.73-0.015T$
Zinc	$126.67-0.060T$	$24.63+0.060T$	$375.69+0.18T$	479.89

Table 4
Comparison between the experimental thermal conditions

Thermophysical properties		Unit	Tin	Lead	Zinc
Initial substrate temperature	T_s^i	°C	20	20	20
Initial casting temperature	T_c^i	°C	300	420	541
Melting temperature	T_c^m	°C	232	327	420
Superheat ΔT	$T_c^i - T_c^m$	°C	68	94	121
Latent heat	L	kJ kg^{-1}	59	24.8	112
Specific heat at T_c^i	C_p^i	J kg^{-1} K^{-1}	243	146	479
Contact angle on nickel substrate	θ	°	40	48	—
Surface tension at T_c^m	σ	Nm^{-1}	0.46	0.54	0.78
Dynamic viscosity at T_c^m	μ	Pas $\times 10^{+3}$	2.71	2.10	3.17
Substrate roughness	R_a	μm	15.58	15.58	15.58
Solidified metal roughness	R_a	μm	13.69	12.27	7.87
Stefan number	$St = \frac{Cp^i \Delta T}{L}$	—	0.28	0.59	0.52

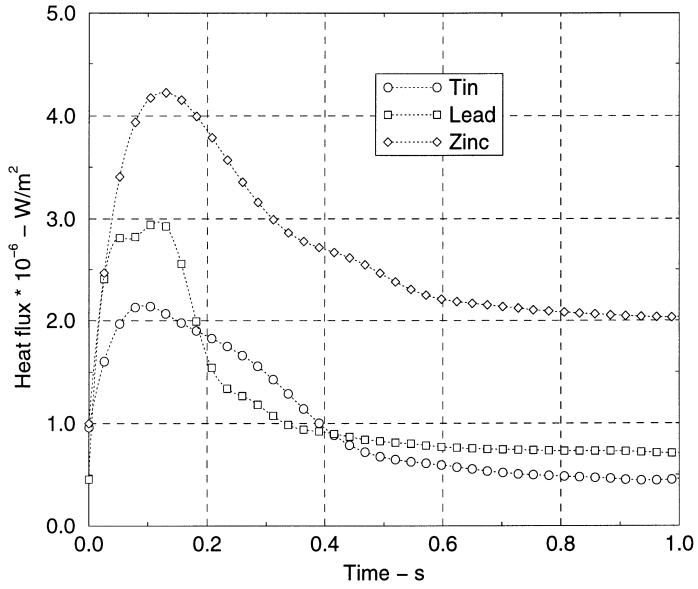

Fig. 12. Heat flux evolution vs nature of metal.

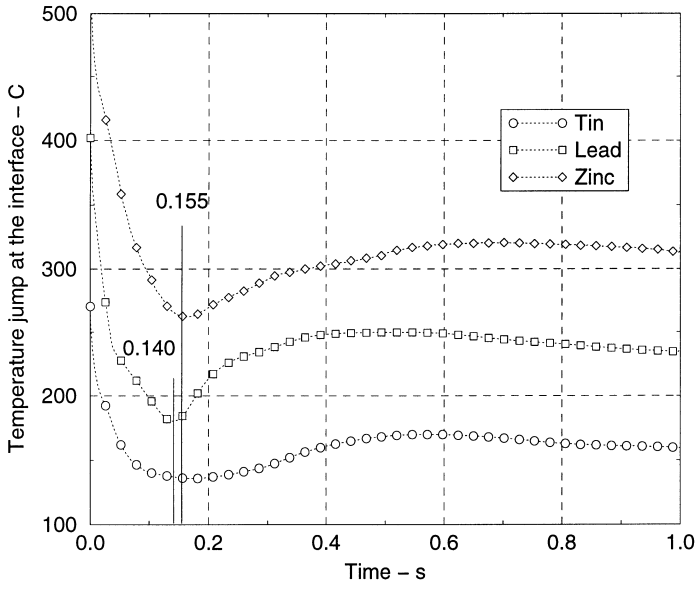

Fig. 13. The jump temperature at the interface as function of metal nature.

taking into consideration the competition between superheat energy $C_p(T_c^i - T_f)$ and latent heat energy characterized by the Stefan number (St). The values of this number are also given in Table 4. It can be seen that the Stefan number is approximately the same for lead and zinc. However, the behaviour for lead and zinc is different. This means that this Stefan number is not sufficient to control the behavior of thermal contact conditions in the stage **C**. Moreover, the influence of solidification rate and volume change can be analyzed in considering the time where the solidification front reaches the sensor installed in casting and the value of contraction parameter ρ^*; see Table 4. It appears that this time is the same for tin and lead and twice for the case of zinc. It means that the buckling and shrinkage phenomena, due to the volume change, must occur later in zinc.

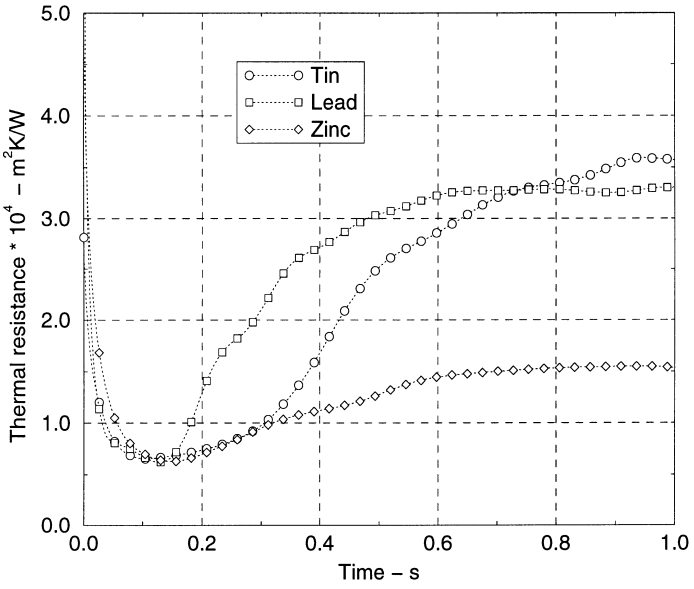

Fig. 14. Thermal contact resistance evolution as function of metal nature.

4. Conclusion

An experimental setup was used to investigate the solidification, cooling and thermal contact conditions of small molten metal drops spreading on solid substrate. A fine instrumentation was used to record temperature histories on both sides: casting and substrate. The simple numerical procedure developed for measurements processing [12] is validated experimentally.

The study has been developed to understand the fundamental heat transfer mechanisms at the casting-substrate interface. A parametric study has been performed using our experimental setup. The effect of various processing variables, such as melt superheat, substrate roughness, lubricant type and melt materials. Three pure molten metals were used (tin, lead and zinc) with various melt superheat in the case of tin. Three substrates with the same material (nickel) but with various surface roughness were used.

Step-wise variation of the thermal contact resistance, during the solidification process has been proposed and analyzed, step **A** covering the earlier stages of molten metal-substrate contact and the period of liquid metal cooling; step **B** representing the established contact period and the beginning solidification process; setup **C** representing the growth of the solidification process and the cooling phase in the casting region. This thermal analysis can be used to build an empirical model for the prediction of thermal contact resistance and heat flux at the interface. It comes from the above analysis, that the model must take into account the thermophysical properties of mold and casting.

The obtained results, for the same metal, indicate that the increase of superheat improves the wettability of the substrate surface and provokes a decreasing of the thermal contact resistance. The effect of lubricant type at the interface was also found to be important. The presence at the interface of a better thermal conductor than air leads to high quality of heat transfer. The cooling rate of solidifying metals is closely related to their latent heat and superheat. It is seen that the highest latent heat, the lowest thermal contact resistance. The surface tension and contact angle have also the same effect. The highest surface tension and contact angle the lowest wettability solidified metal.

Looking to the literature, the numerical and experimental procedure developed in this study seem to give a good estimate of thermal contact conditions during the solidification process. All factors mentioned are going to increase the complexity of thermal contact resistance in metal casting. Furthers investigations should be done to analyze further the effect of these factors.

References

[1] A.V. Reddy, C. Beckermann, Measurement of metal–mold interfacial heat transfer coefficient during solidification of sn and sn–pb alloys, Experimental Heat Transfer 6 (1993) 111–129.
[2] A. Garcia, T.W. Clyne, M. Prates, Mathematical model of the undirectional solidification of metals: I. Cooled molds, Metallurgical Transactions B 9 B (1978) 449–457.
[3] C.G. Levi, R. Mehrabian, Heat flow during rapid solidifica-

tion of undercooled metal droplets, Metallurgical Transactions A 13 A (1982) 221–234.
[4] C.A. Muojekwu, I.V. Samaresekera, J.K. Brimacombe, Heat transfer and microstructure during the early stages of metal solidification, Metallurgical and Materials Transactions B 26 B (1995) 361–382.
[5] J. Issac, G.R. Reddy, G.K. Sharma, Numerical simulation of solidification of castings in metallic molds, AFS Transactions 85 (1985) 123–132.
[6] A. Garcia, T.W. Clyne, M. Prates, Mathematical model for the undirectional solidification of metals: II. Massive molds, Metallurgical Transactions B 10 B (1979) 85–92.
[7] J.G. Henzel, J. Keverian, Gap formation in permanent mold casting, AFS Transactions 68 (1960) 373–379.
[8] R.C. Sun, Simulation and study of surface conductance for heat flow in the early stage of casting, Cast Metal Research Journal 6 (3) (1970) 105–110.
[9] L.J.D. Sully, The thermal interface between castings and chill molds, AFS Transactions 84 (1976) 735–744.
[10] C.G. Levi, The evolution of microcrystalline structures in supercooled metal powders, Metallurgical Transactions A 19 A (1989) 699–708.
[11] J.K. Brimacombe, I.V. Samaresekera, Fundamental aspects of the continuous casting of near-net-shape steel products, in: R.S. Carbonara, Y. Sahai, J.E. Battles, C.E. Mobley, (Eds), Casting of Near Net Shape Products, The Metallurgical Society, 1988, pp. 3–24.
[12] T. Loulou, E.A. Artyukhin, J.P. Bardon, Estimation of thermal contact resistance during the metal solidification process: I—experiment principle and modelisation, Int. J. Heat Mass Transfer 42 (1999) 2119–2127.
[13] J.P. Bardon, Mesure de température et de flux de chaleur par des méthodes par contact, Proc. de l'Ecole de Printemps METTI, 1: 3.1–3.22, Mars 1995, pp. 19–25.
[14] J.P. Bardon, Température de surface, mesure par contact, Techniques de l'Ingénieur, Traité Mesures et Contrôle, Grandeurs Thermiques, Part R5II: R 2732/1–4, 1988.
[15] B. Cassagne, J.P. Bardon, J.V. Beck, Theoritical and experimental analysis of two surface thermocouples, in: Proceedings of the Eighth Conference on Heat and Mass Transfer, vol. 2, Hemisphere Publishing Corp., Washington D.C., 1986, pp. 483–488.
[16] K. Ho, R.D. Pehlke, Mechanisms of heat transfer at a metal–mold interface, AFS Transactions 92 (1984) 587–598.
[17] K. Ho, R.D. Pehlke, Metal–mold interfacial heat transfer, Metall. Transaction 16 B (1985) 585–596.
[18] T. Loulou, E.A. Artyukhin, J.P. Bardon, Solidification of molten tin drop on a nickel substrate, in Proceedings of Tenth International Heat Transfer Conference, vol. 4, Brighton, U.K., August 1994, pp. 73–78.
[19] M. Prates, H. Biloni, Variables affecting the nature of the chill zone, Metall. Trans. 3 (1972) 1501–1510.
[20] J.V. Naidich, Progress in Surface and Membrane Science, Academic Press, New York, 1981.